ASEAN Journal for Science and Engineering in Materials

Journal homepage: https://ejournal.bumipublikasinusantara.id/index.php/ajsem

Fabrication of Synthetic Lumbar Vertebrae by a Combination of FDM 3D-Printing and PU Foam Casting from Two Injection Techniques for Surgical Training

Farid Triawan[1,], Nisa Khoiriyah[1], Asriyanti[1], Muhammad Satrio Utomo[2,3], Kushendarsyah Saptaji[1], Nikolas Krisma Hadi Fernandez[1], Muhammad Akhsin Muflikhun[4]*

[1]Sampoerna University, Jakarta, Indonesia
[2]National Research and Innovation Agency, Banten, Indonesia
[3]University of Melbourne, Melbourne, Australia
[4]Universitas Gajah Mada, Yogyakarta, Indonesia
Correspondence: E-mail: farid.triawan@sampoernauniversity.ac.id

ABSTRACT

This study aims to introduce a rapid and precise fabrication technique of lumbar vertebrae model that mimics the cortical and cancellous parts of the bone using polylactic acid (PLA) and polyurethane (PU) foam, respectively. An FDM 3D-printing using PLA filament was utilized to fabricate the cortical part, then PU foam was molded into the printed cortical to form the cancellous part. The fabricated model was examined by comparing its dimensions with the stereolithography (STL) model. Sequentially, density measurement, compressive test, and microstructure observation were performed to evaluate the specimen characteristics. The results showed that the dimensions of the vertebrae model agreed well with the STL model, with a discrepancy of less than 4%. The fabricated PU samples exhibited a density in the range of 476–557 kg/m³, elastic moduli of 3.99–7.17 MPa, and a pore size of 136.66–179.80 µm, which are lower than the properties of human bone. Despite that, the PU samples maintain their compressive strength of 0.329–0.589 MPa, which is within the range of cancellous human bone.

ARTICLE INFO

Article History:
Submitted/Received 02 Feb 2025
First Revised 01 Mar 2025
Accepted 27 May 2025
First Available online 28 May 2025
Publication Date 01 Mar 2026

Keyword:
3D printing,
Lumbar,
Polyurethane foam,
Surgical training,
Synthetic bone.

1. INTRODUCTION

The lumbar spine plays a vital role in human activity, where it has superior rigidity and functionality compared to cervical and thoracic bones (Saad *et al*., 2020; Galbusera & Bassani, 2019; Sparrey *et al*., 2014). However, it shows that 80% of people are affected by spinal degeneration (Frost *et al*., 2019; Ravindra *et al*., 2018; Teraguchi *et al*., 2014), which requires a highly skilled surgeon for treatment. Lack of skills during treatment may lead to problems, such as necrosis due to excessive heat generation, fracture pedicle, and cracks in the structure (Lughmani *et al*., 2015). These surgical skills can be enhanced through surgical training programs to familiarize the surgeon with basic surgical maneuvers (Atesok *et al*., 2012; Ruikar *et al*., 2018; Moles *et al*., 2009). The training program requires models to give tactile feedback, which is important since precise tactile feedback will give an accurate and intuitive sensation to the trainee (Liu *et al*., 2024; Shull & Damian, 2015). Besides, tactile feedback also gives the impression of the quality of the bone, which can be crucial when doing surgery (Wang *et al*., 2022).

Two types of models can be used for training purposes, which are cadaver specimens and synthetic models. Cadaver specimens give the best feedback during training sessions, but are limited, hard to maintain, and expensive (Clifton *et al*., 2019). The alternative is synthetic models, which include Sawbones (US), Creaplast (France), and Synbone (Switzerland). However, the commercial product is usually too light to represent and to mimic the tactile feeling while cutting and drilling the structure of the bone model (Blair-Pattison, 2016). Besides, those products usually only consist of one material that cannot mimic the transition of cortical and cancellous models of the bone. Therefore, having a model that uses heterogeneous material at the same time to mimic both the cortical and cancellous types can help the trainers to experience the tactile and transition feedback while processing the model (Kang *et al*., 2008).

The current trend involves using additive manufacturing (AM) for medical modeling to prepare and train clinicians (Ghomi *et al*., 2021; Garg & Mehta, 2018). Other studies (Bohl *et al*., 2019) focused on using 3D printing for creating the cortical and cancellous transition by printing ABS filament with several shells or thickness equal to 4 and infill density of 20%. The study showed that using the proposed model helped the trainer increase their practical assessment score. Some researchers (Clifton *et al*., 2020) highlighted the use of PLA and PVA filaments to represent the cortical and cancellous parts. This combination accurately gave the tactile feedback during pedicle probing, tapping, and screw placing. However, the model did not mimic the complex characteristics of human vertebrae. Other reports (Asriyanti *et al*., 2022) highlighted the use of rigid polyurethane (PU) foam as the material to fabricate a lumbar spine model using an indirect 3D printing method. They also focused on the parameters of the casting process to fabricate the PU foam, which helps the fabrication process of PU foam in the current study. Although the study introduced model integrity, it did not discuss the fabrication process and properties of the combined materials in detail.

This study aims to introduce a fabrication method of synthetic lumbar vertebrae by combining Fused Deposition Modelling (FDM) 3D-printing and PU foam casting. FDM is one of the most popular methods for 3D printing models (Ergene *et al*., 2021), including bone models. FDM enables control in the materials, designs, microstructure, and macrostructure through the variation in processing parameters (Houben *et al*., 2017). As for the materials, PLA was chosen to model the cortical section of the bone due to its properties that fall within the modulus of cortical bone affordability, availability, and a straightforward process (Senra & Marques, 2020; Husemoglu *et al*., 2020; Nery *et al*., 2021). On the other hand, PU foam was chosen to model the cancellous part of the bone due to its similarity to human cancellous bone properties (Heiner & Brown, 2001). Besides, PU foam is the standard material for testing orthopaedic devices based on ASTM F1839. Finally, this adds new information regarding the 3D technology as reported elsewhere (Triawan *et* al., 2021; Metteb *et* al., 2025; Shabudin *et* al., 2022).

2. METHOD
2.1. Specimen Fabrications

The fabrication process of the lumbar vertebrae specimen is shown in **Figure 1**. The process began by acquiring a CT scan of the patient's bone model. This scan was converted into a 3D model using DICOM files, which were then meshed and modified into CAD software. The 3D model was exported as an STL model and printed with a 0% infill by FDM 3D printing with a 1.75 mm PLA filament (eSUN) to create the cortical shell. The printer used in this work was Flashforge Creator Pro. There were four sample conditions, which had two types of extruder temperature and thickness as described in **Table 1**. Each of the sample conditions was fabricated three times to obtain the standard deviation from each performance testing per sample condition.

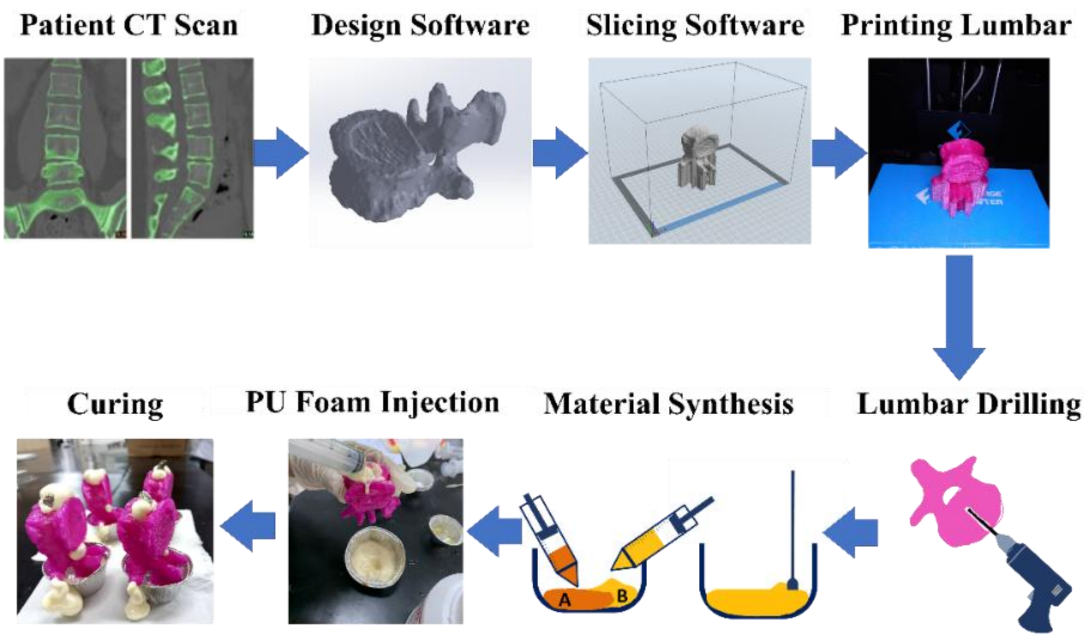

Figure 1. Workflow of the lumbar vertebrae model fabrication process.

Table 1. Printing parameters for the shell structure.

Sample Conditions	Parameters	
	Extruder Temperature (°C)	Thickness (mm)
1	205	1.2
2	205	1.6
3	220	1.2
4	220	1.6

After the shell was printed, it was drilled to create entry and exit holes for PU foam injection. The location of the drilling hole was determined to compensate for PU foam filling and flowing. There are two locations of injection and an excess hole, which were the front and top of the lumbar vertebrae model, as shown in **Figure 2(a)** and **Figure 2(b)**, respectively. The PU foam was synthesized by volumetrically mixing isocyanate and polyol according to the parameters stated in **Table 2**. Subsequently, the mixed PU foam was directly injected into the cortical shell structure via the reaction injection molding (RIM) technique (Lee *et al*., 2002). Due to the nature of the material, PU tends to solidify faster, which makes the material's viscosity go through a rapid transition. The crucial time for casting PU is within 3.16 minutes following the reactant combination (Schäfer *et al*., 2020). However, in this study, the cast was allowed to cure for 24 hours before testing and characterization.

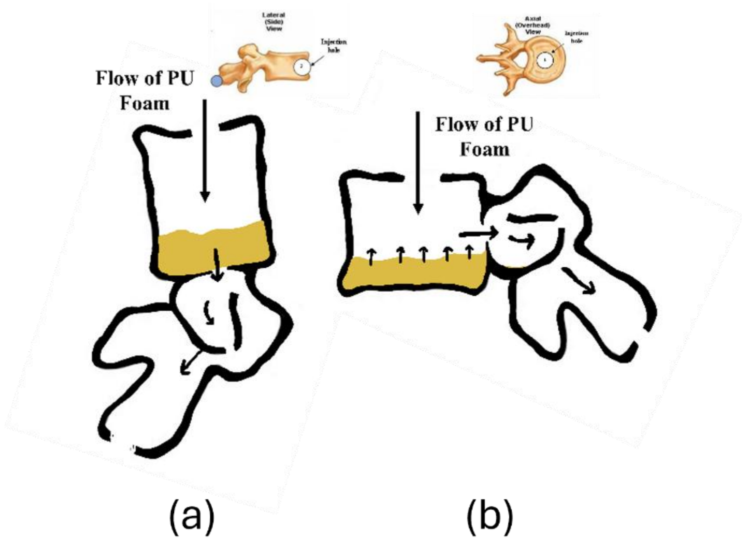

Figure 2. Flow of the PU foam through two different injections and excess holes: (a) front and (b) top side.

Table 2. Parameters of PU mixing.

No.	Parameters	Quantity
1	Isocyanate component	6 mL
2	Polyol component	12 mL
3	Mixing duration	2.5 mins

2.2. Testing and Characterization
2.2.1. Geometry validation

To validate the geometry of the specimens, measurements were taken both before and after PU foam casting. The dimensions of the printed samples were compared to those of the original STL model. Given the complex shape of the lumbar vertebrae, only specific points were selected for measurement. These points corresponded to areas of critical importance during spinal fusion surgery, as illustrated in **Figure 3** (Reid *et al*., 2019). The measurements were done three times, as stated in **Table 3**, in the following locations: maximum distance between transverse processes (TDm), articular processes (Adm), pedicle width (PW), pedicle height (PH), and middle end-plate depth (EPDm). A vernier caliper (Mitutoyo) was used to measure the distances between these points on the physical models. The dimensions or geometry of the samples were considered valid if the discrepancy or the gap error between the samples and the STL model was lower than 5%.

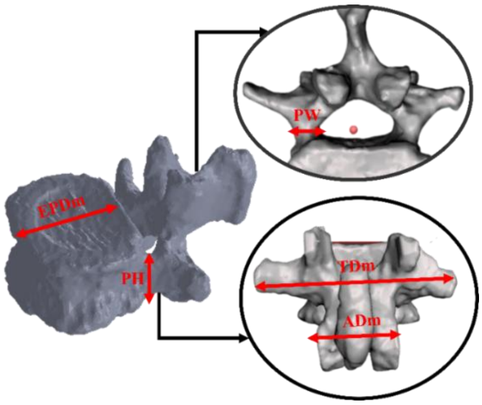

Figure 3. Landmark notation in the lumbar model.

2.2.2. Density measurement

Density is a crucial factor in determining the suitability of the lumbar vertebrae model for surgical training. Higher density material provides more realistic tactile feedback during training, which can be correlated with mechanical properties such as compressive strength. To assess the suitability of the lumbar vertebrae model, the density was measured three times, as stated in **Table 3,** and compared to that of a typical human bone. The mass of the printed and cast lumbar vertebrae model was determined using a digital mass balance (KERN EW 2200-2NM, KERN). The volume was calculated using Meshmixer (Autodesk, Inc.). Finally, the density was evaluated according to ASTM D1622/D1622M-14.

2.2.3. Compression test

To evaluate the compressive properties of the lumbar vertebrae samples and compare them with those of typical human bone, compression tests were conducted using a 313 Family Universal Testing Machine (TestResources Inc.). Two types of compression tests were performed: one on PU foam samples and the other on composite PLA–PU foam samples. The PU foam samples were cube-shaped, as shown in **Figure 4(a)**, and were prepared by cutting the cast PU foam into cubes measuring 25.4 mm on each side. A load of 2 kN was applied during testing, following ASTM D1621-16. For the combined PLA-PU foam samples, testing was performed according to ASTM D695-02a in a cylindrical shape, as illustrated in **Figure 4(b)**. The combined PLA-PU foam samples had a diameter of 12 mm and a height of 25 mm. A compression load of 35 kN was applied at a rate of 1.5 mm/min. Each sample type was tested three times, as summarized in **Table 3**.

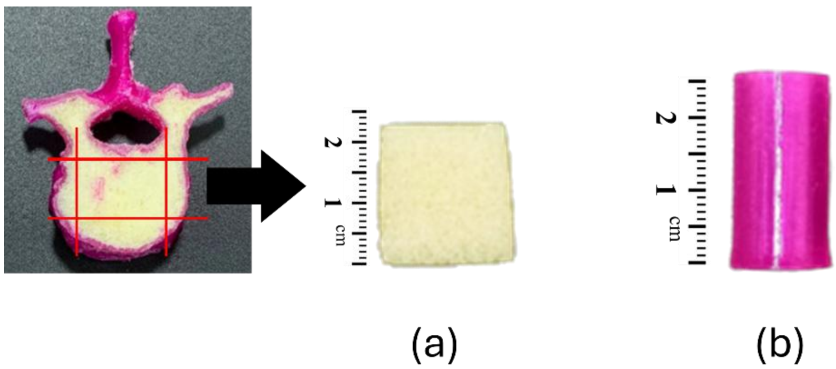

Figure 4. Sample for compression tests: (a) PU foam and (b) combined materials.

Table 3. Number of samples for each test.

No.	Sample	Number of samples			
		Geometry validation	Density measurement	Compression test	Microstructure characteristics
1	PLA-PU combined	3	3	3	—
2	PU foam	—	—	3	3

2.2.4. Microstructure characteristics

The microstructure of the samples, particularly pore size, influences both the overall weight and mechanical strength. A bone-like microstructure can help reduce weight while maintaining the required strength (Syahrom *et al*., 2015). Microstructural analysis was performed on PU foam samples taken from the same cast used for the compression test, as shown in **Figure 4**. The measurement was done three times, as stated in **Table 3**. The analysis involved slicing the sample and observing it using a GAOSUO digital microscope at 40× magnification. Images were captured and processed using ImageJ to evaluate the pore diameter and distribution within the sample. The measured pore diameters were then compared to those of typical human bone.

3. RESULTS AND DISCUSSION

3.1. Fabrication of the Lumbar Model

Figure 5 shows the fabricated lumbar vertebrae samples. The pink color is the cortical shell, and the yellowish color is the cast PU foam. The yellowing color on the PU foam is due to air and light exposure (Parsons & Mountain, 2007) and chemical changes in a polymer that exhibits aromatic structure on the foam (La Nasa *et al*., 2018). Besides, the yellowing phenomenon also occurred due to thermal degradation during crosslinking (La Nasa *et al*., 2018). **Figure 5(a)** shows that the pore size of the PU is smaller when the injection hole is located in front of the vertebral body. Moreover, this variation can make all the PU evenly distributed in all the cavities inside the shell. On the other hand, the filling pattern when using the injection hole located at the top of the vertebral body has a non-uniform pore size inside the shell, as shown in **Figure 5(b)**. Besides, the location near the pedicle body and the spinous isocyanate component is not filled by the PU foam. Based on the result, the location of the injection hole in front of the vertebral body is selected and suggested for fabricating the lumbar model.

Previous research mentioned the importance of gravity in locating the PU foam in the mold (Özdemir & Akar, 2018). Right after the injection of PU foam, the material will immediately buckle down due to gravity. This made the material in contact with the molding part. Setting the location for injecting the PU foam, as in **Figure 5(a)**, will make the PU flow faster due to the gravitational effect. Before the bubble grows, the material moves directly in the direction of gravity. In the casting process, the material will spread in all directions (Özdemir & Akar, 2018). For the injection hole located at the top, the material experienced foaming for a while, then it would flow to the spinous and transverse part in **Figure 2(b).** This will make the travelling time for the material longer. As the duration gets longer, the viscosity of the material increases, and it makes the PU foam unable to flow further. Consequently, the cavity in several parts is not filled. Maintaining the material has low viscosity is essential to ensure the redistributed material inside the mold (Geier *et al*., 2009).

Besides unfilled cavities, the material also experiences another issue, such as pore distribution. During the injection process, there is a possibility that the air goes into the shell together with the PU material. When the injection hole was placed in the top, this air could be trapped and stay in the vertebral body due to the absence of an excess hole. This caused the air bubbles trapped in the foam (Özdemir & Akar, 2018). The entrapped air was also caused by the increasing amount of air pressure (Samkhaniani *et al*., 2013).

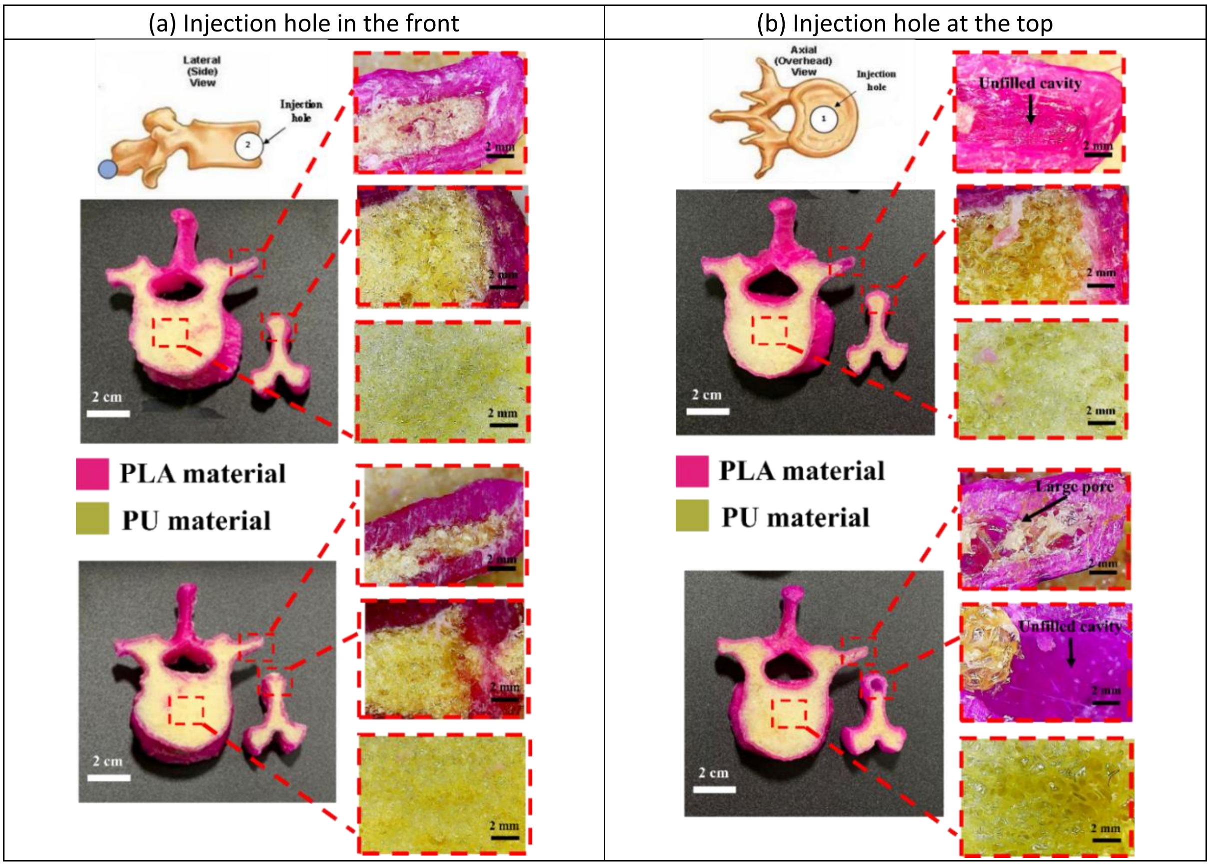

Figure 5. Mold filling pattern inside the lumbar shell with injection hole variation for injection hole (a) in the front and (b) at the top.

3.2. Characterization Results
3.2.1. Geometry validation

The results in **Figure 6** show the geometric discrepancies of the fabricated samples with the STL model before and after casting. It is found that the sample's dimensions are generally bigger than the dimensions of the STL model. For example, the TDm part showed a discrepancy of less than 2% before the casting process, then it became a bit larger after the casting process, with a discrepancy of 2.23%. For the ADm part, a similar tendency was observed, in which both samples of before and after casting were larger than the STL model, with a discrepancy of less than 4%. Interestingly, a dramatic change in dimensions was observed in the before and after casting in sample condition 3, which had a discrepancy from 0.36 to 3.51%. Nevertheless, the discrepancy is still lower than 4%. A different phenomenon was observed for the EPDm and PH parts. The samples before casting were smaller (shrinking) compared to the STL model. Then, it became larger compared to the STL model after the casting process.

The discrepancy before casting is likely due to die swelling. This implies that the printer could have extracted more filaments than what was programmed (Alafaghani *et al*., 2017). Whereas the area printed parallel to z- and the y-axis is shrinking. The wrapping or shrinkage in the FDM part is usually induced by uneven heat distribution in the printed part (Alsoufi *et* *al*., 2019). Besides, higher temperatures during printing will decrease the viscosity and fluidity of the filament (Zharylkassyn *et al*., 2021). Lower viscosity decreases the shear stress, which increases the flow of the material in the nozzle (Akbaş *et al*., 2020). This situation causes dripping of the filament during printing. Hence, the extruded material expands and affects the dimensions of the FDM components.

After the casting process, all parts of the sample exhibited an increase in dimensions, which is due to the injected PU foam. The expansion is due to the nature of PU foam that experiences a foaming process, leading to an increase in volume (Sun *et al*., 2021; Liu *et al*., 2023; Al-Atroush & Sebaey, 2021). This phenomenon is more pronounced on samples with higher printed temperatures and thinner shells. This is due to the lower dimensional resistance of the samples with thinner shells to hold the expansions of the PU foam. Despite these expansions, the dimensional discrepancies of all parts on the sample conditions compared to the STL model remain below 4%, which validates the dimensions of the samples.

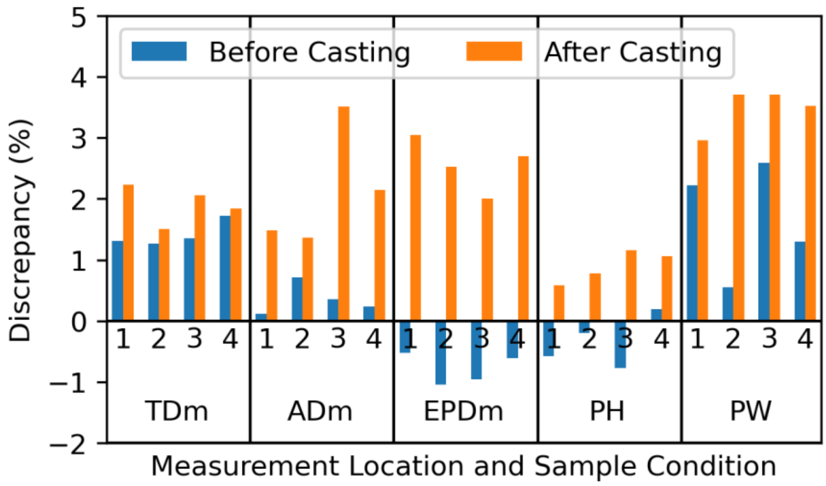

Figure 6. Dimensional discrepancy of the synthetic spinal model relative to the STL model.

3.2.2. Density measurement

A comparison between the density of the PLA-PU combined sample and human bone based on the ASTM standard was performed. The comparison result is shown in **Figure 7**, with the black bar showing the standard deviation of the data. The result shows that the density of PLA and PU foam combined materials that were used in the current study is in the range of 476–557 kg/m^3, below the density of human bone, which has a range of 937–1157 kg/m^3 (Öhman-Mägi *et al*., 2021). Nevertheless, the proposed specimens are still comparable to a commercial bone model that has a nominal density of 240 kg/m^3 (Brown *et al*., 2019).

The area of the pouring size affects the density of the PU foam (Jackovich *et al*., 2005). As the shell increases, the inner area and density decrease. Hence, the lumbar vertebrae models with conditions 2 and 4 have a smaller inner area. This statement is in line with the pore size effect on the thickness of the mold material. As the PU experiences foaming in the closed mold, such as in the printed bone shell, the mold's wall restricts the free flow process, which will generate a packing effect that increases the density (Asriyanti *et al*., 2022; Jackovich *et al*., 2005). Besides, when the inner area gets bigger as condition 1, the density is higher. The higher density indicates that the cell or pore diameter is smaller (Hatchett *et al*., 2007).

3.2.3. Compression test

The stress-strain curve of PU foam is shown in **Figure 8,** while the calculated compressive properties of PU foam are shown in **Table 4**. The results show that the overall strength of the foam increases as the temperature and thickness of the shell increase. In contrast, the elastic moduli tend to decrease as the temperature and shell thickness increase, with sample condition 1 having the closest compressive modulus. In addition, the compressive strength is in the range of 0.329–0.589 MPa, which is in the range of a typical cancellous part of human bone. However, the compressive modulus is in the range of 3.990–7.172 MPa, lower than that of the human bone. The typical compressive strength and modulus for cancellous human bone are in a range of 0.1–30 MPa and 10–3000 MPa, respectively (Öhman-Mägi *et al*., 2021; Gerhardt & Boccaccini, 2010; Morgan *et al*., 2018) (see **Table 4**).

The stress-strain curve of the combined PLA-PU foam material is shown in **Figure 9**, while the calculated result for compressive properties is shown in **Table 5**. The result shows that the compressive strength and modulus range from 38.08–45.83 MPa and 1.091–1.213 GPa, respectively. A linear trend between extruder temperature and the thickness of the shell is revealed from the results. When the temperature increases, the compressive properties increase as well. In addition, the thicker printing shell produces higher strength.

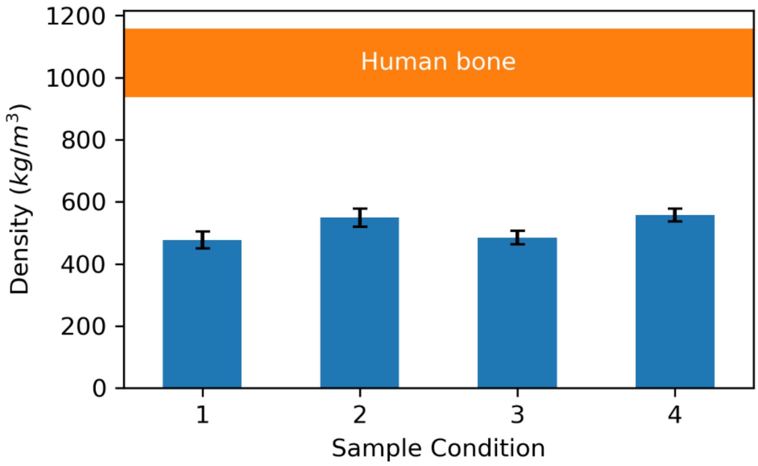

Figure 7. Comparison of the density of PLA-PU combined material in the spinal model.

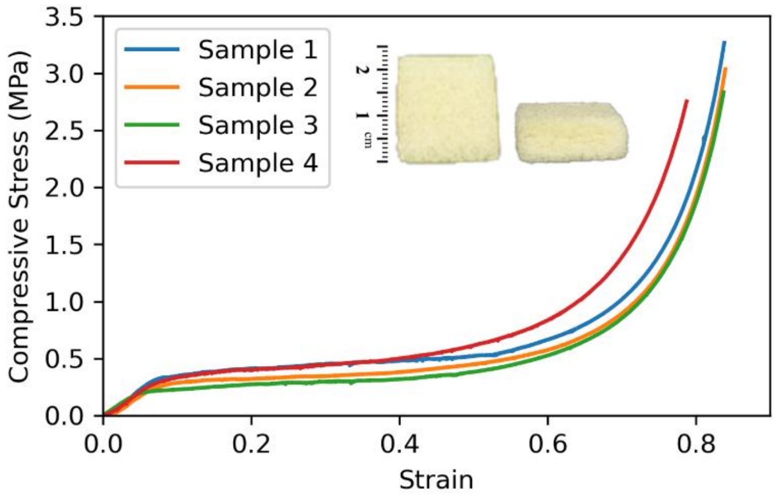

Figure 8. Stress-strain curve of PU foam.

Table 4. Compressive strength and modulus of PU foam.

Sample Condition	Compressive Strength (MPa)	Compressive Modulus (MPa)
Human bone	0.1 - 30	10 – 3000
1	0.589 ± 0.242	7.172 ± 2.408
2	0.412 ± 0.061	5.063 ± 0.315
3	0.329 ± 0.039	4.377 ± 1.038
4	0.480 ± 0.064	3.990 ± 1.636

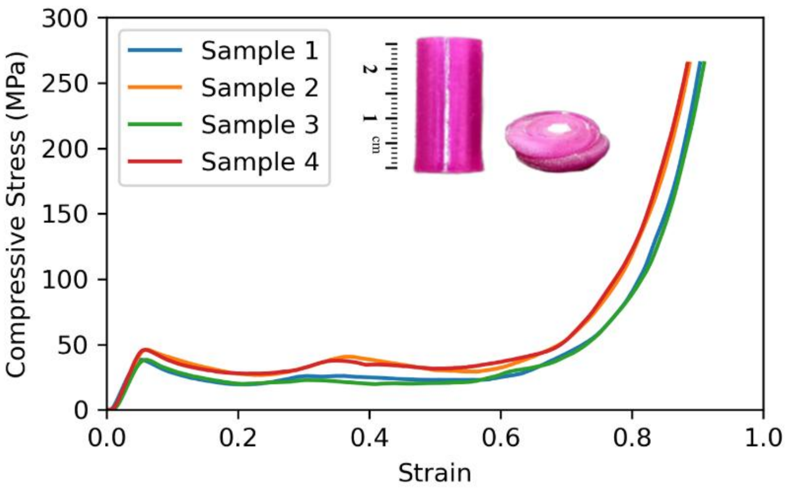

Figure 9. Stress-strain curve of the combined material of PLA-PU foam.

Table 5. Compressive strength and modulus of PLA-PU foam.

Sample Condition	Compressive Strength (MPa)	Compressive Modulus (GPa)
1	38.08 ± 0.50	1.091 ± 0.027
2	43.29 ± 3.76	1.165 ± 0.078
3	41.24 ± 5.12	1.144 ± 0.101
4	45.83 ± 0.21	1.213 ± 0.015

3.2.4. Microstructure characteristics

The pictures of the specimens' microstructure are shown in **Figure 10**, while the measured pore size is presented in **Figure 11**, with the black bar showing the standard deviation for each sample condition. From microscope observation, samples with higher extruder temperatures introduce a smaller pore size. The samples with higher extruder temperature tend to increase the molding area, as mentioned in Section 3.2.1, which then decreases the pore size. This finding goes against the other findings (Rizvi *et al*., 2018), which show that higher molding area increases the pore diameter. Besides, the pore diameter of the samples for all conditions is in a range of 136.66–179.80 µm, lower than the pore diameter of typical human bone, which is about 500–1200 µm (Zhang *et al*., 2024). This difference may affect the properties of the model, including the density, stiffness, strength, and permeability of the model (Syahrom *et al*., 2015; Parsons & Mountain, 2007). Other studies (Seehanam *et al*., 2024) show that the higher pore size of the model could decrease both the initial peak stress and energy absorption.

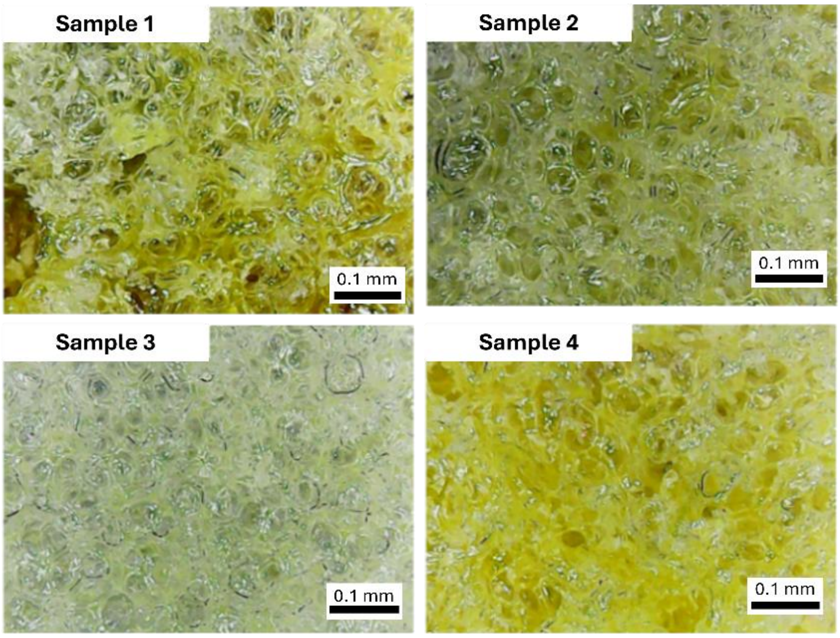

Figure 10. Micrograph of PU foam inside the shell structure with different shell conditions.

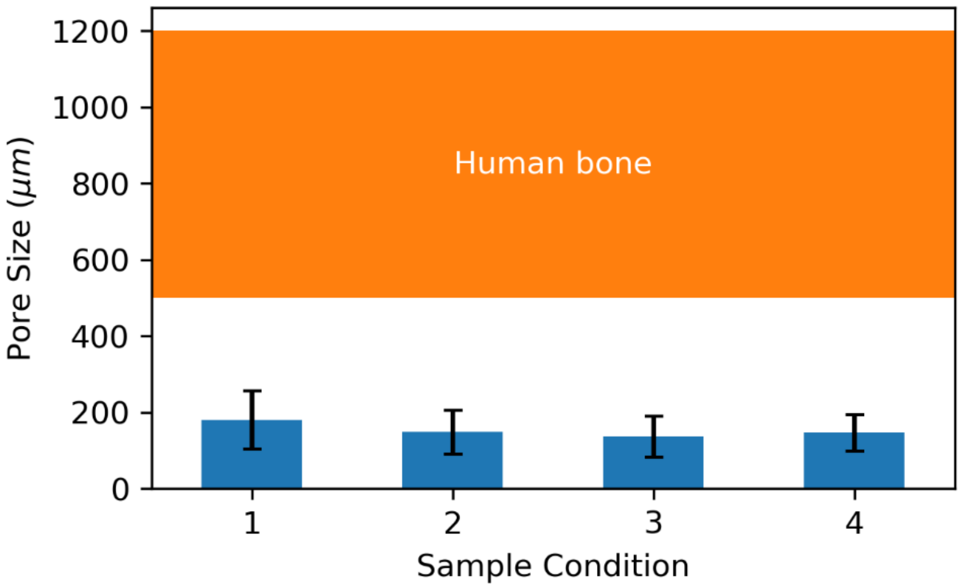

Figure 11. Pore size for each sample condition.

4. CONCLUSION

This research presents the fabrication of synthetic lumbar vertebrae produced by PLA and polyurethane (PU) foam to mimic the cortical and cancellous parts of a human bone. The cortical part is fabricated by 3D printing, while the cancellous part is fabricated by casting the PU foam into the printed cortical shell. Geometric discrepancy of the samples relative to the STL model was below 4%, with a maximum of 2.59% before casting and 3.70% after casting. Then, the density, microstructure, and compressive properties of the model were evaluated and compared to the human bone. The results show that the fabricated PU foam exhibits lower density (476–557 kg/m³) and pore size (137–180 µm) than that of the human cancellous bone (937–1157 kg/m³ and 500–1200 µm for density and pore size, respectively). Similarly, the compressive moduli of the PU samples (3.990–7.172 MPa) are also lower than that of the human bone (10–3000 MPa). However, the compressive strength of the PU samples (0.329–0.589 MPa) is within the range of the properties of cancellous human bone (0.1–30 MPa). The results show a promising methodology for producing lumbar bone models for surgical applications.

5. ACKNOWLEDGMENT

The authors would like to thank Sampoerna University, the National Research and Innovation Agency of Indonesia, and the University of Indonesia for the research facilities and funding used in this research.

6. AUTHORS' NOTE

The authors declare that there is no conflict of interest regarding the publication of this article. Authors confirmed that the paper was free of plagiarism.

7. REFERENCES

Akbaş, O. E., Hıra, O., Hervan, S. Z., Samankan, S., and Altınkaynak, A. (2020). Dimensional accuracy of FDM-printed polymer parts. *Rapid Prototyping Journal*, *26*(2), 288-298.

Alafaghani, A. A., Qattawi, A., Alrawi, B., and Guzman, A. (2017). Experimental optimization of fused deposition modelling processing parameters: a design-for-manufacturing approach. *Procedia Manufacturing*, *10*, 791-803.

Al-Atroush, M. E., and Sebaey, T. A. (2021). Stabilization of expansive soil using hydrophobic polyurethane foam: A review. *Transportation Geotechnics*, *27*, 100494.

Alsoufi, M. S., Alhazmi, M. W., Suker, D. K., Alghamdi, T. A., Sabbagh, R. A., Felemban, M. A., and Bazuhair, F. K. (2019). Experimental characterization of the influence of nozzle temperature in FDM 3D printed pure PLA and advanced PLA+. *American Journal of Mechanical Engineering*, *7*(2), 45-60.

Asriyanti, A., Saptaji, K., Khoiriyah, N., Utomo, M. S., Dwijaya, M. S., Triawan, F., and Nadhif, M. H. (2022). Fabrication of rigid polyurethane foam lumbar spine model for surgical training using indirect additive manufacturing. *International Journal of Technology*, *13*, 1612.

Atesok, K., Mabrey, J. D., Jazrawi, L. M., and Egol, K. A. (2012). Surgical simulation in orthopaedic skills training. *JAAOS-Journal of the American Academy of Orthopaedic Surgeons*, *20*(7), 410-422.

Blair-Pattison, A. (2016). Development and characterization of a synthetic bone analogue for surgical training. *Development*, *2016*, 01-18.

Bohl, M. A., Zhou, J. J., Mooney, M. A., Repp, G. J., Cavallo, C., Nakaji, P., and Kakarla, U. K. (2019). The Barrow Biomimetic Spine: effect of a 3-Dimensional-Printed spinal osteotomy model on performance of spinal osteotomies by medical students and interns. *Journal of Spine Surgery*, *5*(1), 58.

Brown, A. D., Walters, J. B., Zhang, Y. X., Saadatfar, M., Escobedo-Diaz, J. P., and Hazell, P. J. (2019). The mechanical response of commercially available bone simulants for quasi-static and dynamic loading. *Journal of the Mechanical Behavior of Biomedical Materials*, *90*, 404-416.

Clifton, W., Nottmeier, E., Damon, A., Dove, C., Chen, S. G., Pichelmann, M., & Chen, S. (2019). A feasibility study for the production of three-dimensional-printed spine models using simultaneously extruded thermoplastic polymers. *Cureus*, *11*(4), 1-6.

Clifton, W., Pichelmann, M., Vlasak, A., Damon, A., ReFaey, K., and Nottmeier, E. (2020). Investigation and feasibility of combined 3D printed thermoplastic filament and polymeric foam to simulate the corticocancellous interface of human vertebrae. *Scientific Reports*, *10*(1), 2912.

Ergene, B., ŞEKEROĞLU, İ., Bolat, Ç., and Yalçın, B. (2021). An experimental investigation on mechanical performances of 3D printed lightweight ABS pipes with different cellular wall thickness. *Journal of Mechanical Engineering and Sciences*, *15*(2), 8169-8177.

Frost, B. A., Camarero-Espinosa, S., and Foster, E. J. (2019). Materials for the spine: anatomy, problems, and solutions. *Materials*, *12*(2), 253.

Galbusera, F., and Bassani, T. (2019). The spine: a strong, stable, and flexible structure with biomimetics potential. *Biomimetics*, *4*(3), 60.

Garg, B., and Mehta, N. (2018). Current status of 3D printing in spine surgery. *Journal of Clinical Orthopaedics and Trauma*, *9*(3), 218-225.

Geier, S., Winkler, C., and Piesche, M. (2009). Numerical simulation of mold filling processes with polyurethane foams. *Chemical Engineering & Technology: Industrial Chemistry-Plant Equipment-Process Engineering-Biotechnology*, *32*(9), 1438-1447.

Gerhardt, L. C., and Boccaccini, A. R. (2010). Bioactive glass and glass-ceramic scaffolds for bone tissue engineering. *Materials*, *3*(7), 3867-3910.

Ghomi, E. R., Khosravi, F., Neisiany, R. E., Singh, S., and Ramakrishna, S. (2021). Future of additive manufacturing in healthcare. *Current Opinion in Biomedical Engineering*, *17*, 100255.

Hatchett, D. W., Kinyanjui, J. M., and Sapochak, L. (2007). FTIR analysis of chemical gradients in thermally processed molded polyurethane foam. *Journal of Cellular Plastics*, *43*(3), 183-196.

Heiner, A. D., and Brown, T. D. (2001). Structural properties of a new design of composite replicate femurs and tibias. *Journal of Biomechanics*, *34*(6), 773-781.

Houben, A., Van Hoorick, J., Van Erps, J., Thienpont, H., Van Vlierberghe, S., and Dubruel, P. (2017). Indirect rapid prototyping: opening up unprecedented opportunities in scaffold design and applications. *Annals of Biomedical Engineering*, *45*, 58-83.

Husemoglu, R. B., Baysan, G., Ertugruloglu, P., Yücel, A. T., and Havıtçıoğlu, H. (2020). The mechanical comparison of artificial bone and 3D printed bone segments. *Journal of Medical Innovation and Technology*, *2*(2), 127-130.

Jackovich, D., O'toole, B., Hawkins, M. C., and Sapochak, L. (2005). Temperature and mold size effects on physical and mechanical properties of a polyurethane foam. *Journal of Cellular Plastics*, *41*(2), 153-168.

Kang, S. W., Yang, H. S., Seo, S. W., Han, D. K., and Kim, B. S. (2008). Apatite-coated poly (lactic-co-glycolic acid) microspheres as an injectable scaffold for bone tissue engineering. *Journal of Biomedical Materials Research Part A*, *85*(3), 747-756.

La Nasa, J., Biale, G., Ferriani, B., Colombini, M. P., and Modugno, F. (2018). A pyrolysis approach for characterizing and assessing degradation of polyurethane foam in cultural heritage objects. *Journal of Analytical and Applied Pyrolysis*, *134*, 562-572.

Lee, W. H., Lee, S. W., Kang, T. J., Chung, K., and Youn, J. R. (2002). Processing of polyurethane/polystyrene hybrid foam and numerical simulation. *Fibers and Polymers*, *3*, 159-168.

Liu, G., Liao, H., Zhao, X., Liao, W. H., and Cao, J. (2024). Haptic device and interface to reproduce force and tactile feedback of biological tissues. *Sensors and Actuators A: Physical*, *366*, 115022.

Liu, W., Zhang, S., Li, Y., and Ye, X. (2023). The expansion and mechanical property-based cavity expansion model for polyurethane grouting underneath the airport pavement. *Transportation Geotechnics*, *43*, 101141.

Lughmani, W. A., Bouazza-Marouf, K., and Ashcroft, I. (2015). Drilling in cortical bone: a finite element model and experimental investigations. *Journal of The Mechanical Behavior of Biomedical Materials*, *42*, 32-42.

Moles, J. J., Connelly, P. E., Sarti, E. E., and Baredes, S. (2009). Establishing a training program for residents in robotic surgery. *The Laryngoscope*, *119*(10), 1927-1931.

Morgan, E. F., Unnikrisnan, G. U., and Hussein, A. I. (2018). Bone mechanical properties in healthy and diseased states. *Annual review of Biomedical Engineering*, *20*(1), 119-143.

Nery, B., Rivero, L. R., Camporeze, B., Costa, R. A. F., Pereira, L. C., Quaggio, E., and Nery, C. S. A. (2021). Use of three-dimensional reconstruction in 3D molds as an adjuvant in the treatment of cranial and spinal pathologies: technical details and case report. *Interdisciplinary Neurosurgery*, *24*, 100953.

Öhman-Mägi, C., Holub, O., Wu, D., Hall, R. M., and Persson, C. (2021). Density and mechanical properties of vertebral trabecular bone—A review. *JOR Spine*, *4*(4), e1176.

Özdemir, İ. B., and Akar, F. (2018). 3D simulation of polyurethane foam injection and reacting mold flow in a complex geometry. *Heat and Mass Transfer*, *54*(5), 1281-1288.

Parsons, N. S., and Mountain, C. A. (2007). Investigating polyurethane foam as a form of trace evidence. *Science & Justice*, *47*(1), 24-33.

Ravindra, V. M., Senglaub, S. S., Rattani, A., Dewan, M. C., Härtl, R., Bisson, E., and Shrime, M. G. (2018). Degenerative lumbar spine disease: estimating global incidence and worldwide volume. *Global Spine Journal*, *8*(8), 784-794.

Reid, P. C., Morr, S., and Kaiser, M. G. (2019). State of the union: a review of lumbar fusion indications and techniques for degenerative spine disease: JNSPG 75th Anniversary Invited Review Article. *Journal of Neurosurgery: Spine*, *31*(1), 1-14.

Rizvi, A., Chu, R. K., and Park, C. B. (2018). Scalable fabrication of thermally insulating mechanically resilient hierarchically porous polymer foams. *ACS Applied Materials & Interfaces*, *10*(44), 38410-38417.

Ruikar, D. D., Hegadi, R. S., and Santosh, K. C. (2018). A systematic review on orthopedic simulators for psycho-motor skill and surgical procedure training. *Journal of Medical Systems*, *42*, 1-21.

Saad, W. A., Dzahir, M. A. M., Shinichirou, Y., Hussein, M., Mohamad, M., Saad, S. M., and Azaman, A. (2020). Comparison of the spine kinematics by defining lumbar as single and multi-segmental in completing critical daily task. *Journal of Mechanical Engineering and Sciences*, *14*(4), 7600-7608.

Samkhaniani, N., Gharehbaghi, A., and Ahmadi, Z. (2013). Numerical simulation of reaction injection molding with polyurethane foam. *Journal of Cellular Plastics*, *49*(5), 405-421.

Schäfer, K., Nestler, D., Tröltzsch, J., Ireka, I., Niedziela, D., Steiner, K., and Kroll, L. (2020). Numerical studies of the viscosity of reacting polyurethane foam with experimental validation. *Polymers*, *12*(1), 105.

Seehanam, S., Khrueaduangkham, S., Sinthuvanich, C., Sae-Ueng, U., Srimaneepong, V., and Promoppatum, P. (2024). Evaluating the effect of pore size for 3D-printed bone scaffolds. *Heliyon*, *10*(4), e26005.

Senra, M. R., and Marques, M. D. F. V. (2020). Synthetic polymeric materials for bone replacement. *Journal of Composites Science*, *4*(4), 191.

Shull, P. B., and Damian, D. D. (2015). Haptic wearables as sensory replacement, sensory augmentation and trainer–a review. *Journal of Neuroengineering and Rehabilitation*, *12*, 1-13.

Sparrey, C. J., Bailey, J. F., Safaee, M., Clark, A. J., Lafage, V., Schwab, F., and Ames, C. P. (2014). Etiology of lumbar lordosis and its pathophysiology: a review of the evolution of lumbar lordosis, and the mechanics and biology of lumbar degeneration. *Neurosurgical Focus*, *36*(5), E1.

Sun, M., Bi, Y., Zhuang, W., Chen, S., Zhao, P., Pang, D., and Zhang, W. (2021). Mechanism of polyurethane binder curing reaction and evaluation of polyurethane mixture properties. *Coatings*, *11*(12), 1454.

Syahrom, A., Kadir, M. R. A., Harun, M. N., and Öchsner, A. (2015). Permeability study of cancellous bone and its idealised structures. *Medical Engineering & Physics*, *37*(1), 77-86.

Teraguchi, M., Yoshimura, N., Hashizume, H., Muraki, S., Yamada, H., Minamide, A., and Yoshida, M. (2014). Prevalence and distribution of intervertebral disc degeneration over the entire spine in a population-based cohort: the Wakayama Spine Study. *Osteoarthritis and Cartilage*, *22*(1), 104-110.

Wang, T. M., Lin, Y. C., Lan, Y. H., and Lin, L. D. (2022). Evaluation of sawbones training protocol in bone quality classification using tactile sensation. *Journal of Dental Sciences*, *17*(2), 897-902.

Zhang, H., Wang, R., Song, Y., Wang, Y., and Hu, Q. (2024). Research on dual-phase composite forming process and platform construction of radial gradient long bone scaffold. *Bioengineering*, *11*(9), 869.

Zharylkassyn, B., Perveen, A., and Talamona, D. (2021). Effect of process parameters and materials on the dimensional accuracy of FDM parts. *Materials Today: Proceedings*, *44*, 1307-1311.